Solar Energy Materials & Solar Cells 115 (2013) 123–128

Contents lists available at SciVerse ScienceDirect

Solar Energy Materials & Solar Cells

journal homepage: www.elsevier.com/locate/solmat

Enhanced stability in polymer solar cells by controlling the electrode work function via modification of indium tin oxide

Soo Won Heo [a], Eui Jin Lee [a], Kee Won Seong [b], Doo Kyung Moon [a,*]

[a] Department of Materials Chemistry and Engineering, Konkuk University, 1 Hwayang-dong, Gwangjin-gu, Seoul 143-701, Korea
[b] Department of Civil Engineering, Konkuk University, 1 Hwayang-dong, Gwangjin-gu, Seoul 143-701, Korea

ARTICLE INFO

Article history:
Received 25 January 2013
Received in revised form
26 March 2013
Accepted 27 March 2013
Available online 24 April 2013

Keywords:
Polymer solar cells(PSCs)
Self-assembly monolayer(SAM)
FOTES
Stability
Work function control

ABSTRACT

To enhance the work function of indium tin oxide (ITO) and make its surface hydrophobic, triethoxy (1H,1H,2H,2H-perfluoro-1-octyl)silane (FOTES) was introduced as a self-assembly monolayer (SAM) material. A polymer solar cell has been fabricated with FOTES–ITO, and due to decreased series resistance (R_S) and increased shunt resistance (R_{SH}), the short circuit current density (J_{SC}), open circuit voltage (V_{OC}), and fill factor (FF) of the optimized device were 9.2 mA/cm^2, 0.63 V and 57.9%, respectively. The calculated power conversion efficiency (PCE) was 3.4%. In addition, the air stability of the fabricated device was improved.

1. Introduction

The renewable, light-weight, and low-cost polymer-fullerene bulk heterojunction solar cells (BHJ PSCs) have received great attention for next-generation solar cells [1–5]. Spin-coating, ink-jet printing, roll-to-roll printing, brush painting, or stamping techniques can be applied to flexible substrates to inexpensively fabricate light-weight, flexible, large-area photovoltaic devices [6–11]. However, at 8–9%, the power conversion efficiency (PCE) of PSCs remains too low for commercialization [12,13]. To enhance the PCE in PSCs, many studies have been conducted, and have involved the synthesis of new narrow-band-gap materials for improving the photon harvesting properties, optimization of the morphology in bulk heterojunction (BHJ) films, interfacial modification for better charge carrier collection, and design of novel device structures [14–17].

Another critical factor for commercialization is improvement of the stability. Many of the studies on how to increase life time have focused on work function control, and the improvement of stability through the modification of the anode. Poly(3,4-ethylene dioxythiophene)/poly(styrene sulfonate) (PEDOT:PSS) is one of the most widely used anode buffer materials in PSCs. It has advantages of easy handling, high transparency, and good conductivity, because it enables the usage of solution processing. In addition, the high work function (5.0 eV or above) is an improvement over the low work function of ITO (4.4–4.7 eV). In this material, however, metal ions penetrate into the photo-active layer after the indium tin oxide (ITO) is corroded by the strongly acidic PSS in the PEDOT:PSS. As a result, due to these metal ions in the photo-active layer acting as quenching sites for dissociated carriers, the long-term stability is reduced [18–20]. In response to this, there have been studies to improve the PCE and stability without using PEDOT:PSS as an anode buffer layer.

Helander et al. reduced the work function of ITO to 6.1 eV by Cl doping, and achieved power efficiency more than twice as high as that of conventional organic light-emitting diodes (OLEDs), by fabricating chlorinated ITO (Cl-ITO)-based OLEDs [21]. However, according to Sun et al., the photovoltaic performance of PSCs with Cl-ITO degrades quickly with time. This is attributed to the reduction of the work function caused by the desorption of Cl from the ITO surface [22]. To fabricate more stable PSCs, there have been studies on the formation of a monolayer using molecules that could be covalently bonded to the substrate surface [23,24].

Kim et al. controlled the work functions of ITO by introducing ITO to a self-assembly monolayer (SAM), which has an electron-donating or withdrawing group as a terminal group [25]. Trichloro(3,3,3-trifluoropropylsilane) was used as a precursor of CF_3-SAM to enable covalent bonding to the substrate surface. A hydroxyl group was formed through Ar-plasma treatment of the ITO surface, and the ITO of the CF_3-ITO fabricated had an increased work function of with an electron withdrawing group. The PCE of the PSC was greater than that of the device without PEDOT:PSS, but there has been no comparison between a CF_3-ITO-based device and a PEDOT:PSS-based device. In addition, the stability characteristics have not been reported either.

In general, as the number of fluorines in the SAM-treated ITO increases, so does the work function [26,27]. To match the work

* Corresponding author. Tel.: +82 2 450 3498; fax: +82 2 444 0765.
E-mail address: dkmoon@konkuk.ac.kr (D.K. Moon).

0927-0248/$ - see front matter © 2013 Elsevier B.V. All rights reserved.
http://dx.doi.org/10.1016/j.solmat.2013.03.034

function of ITO with the highest occupied molecular orbit (HOMO) level (6.2 eV) of the acceptor, phenyl-C_{61}-butyric acid methyl ester (PCBM), triethoxy(1H,1H,2H,2H-perfluoro-1-octyl)silane (FOTES) is used as a SAM precursor. FOTES has abundant fluorine, and rarely experiences desorption from the ITO surface, since it is covalently bonded. In addition, if a catalyst such as nitric acid is used for SAM treatment, it is possible to form a homogeneous monolayer. Therefore, FOTES–ITO has been fabricated and characterized, and the device performance and stability were measured by fabricating FOTES–ITO-based PSCs.

2. Materials and measurements

2.1. Materials

ITO glass from Samsung Corning was used as a transparent electrode (ITO: 170 nm, 10 Ω/sq). PEDOT:PSS (AI 4083) was purchased from Clevios, and poly(3-hexylthiophene) (P3HT), which was used as a donor material in the photoactive layer, was purchased from Rieke metal. PCBM, the acceptor material, was purchased from Nano C. FOTES was bought from Aldrich and used as a SAM precursor. Nitric acid (HNO_3, 61%) was obtained from Dae Jung Chemical & Metals and used as a catalyst. The chemical structure of P3HT, PCBM, and FOTES are shown in Fig. 1(a–c).

2.2. Measurements

All of the thin films were fabricated using a GMC2 spin coater (Gensys), and their thicknesses were measured using an alpha step 500 surface profiler (KLA-Tencor). The morphology of the FOTES–ITO was observed through atomic force microscopy (AFM, PSIA XE-100). The contact angle was measured with a contact-angle meter (KRUSS K6). The work function of ITO and FOTES–ITO were measured and calculated by ultraviolet photoelectron spectroscopy (UPS). UPS spectra were obtained using monochromatized He I radiation ($h\nu$=21.22 eV) from a He-resonance lamp, with an energy resolution of 0.03 eV, as determined from the slope of the Fermi edge of a sputter-cleaned gold sample. The current density–voltage (*J–V*) characteristics of the PSCs were measured using a Keithley 2400 source measure unit. The devices were evaluated at 298 K using a Class A Oriel solar simulator (Oriel 96000 150-W solar simulator) with a xenon lamp that simulates AM 1.5 G irradiation (100 mw/cm^2) from 400 to 1100 nm. The instrument was calibrated with a monocrystalline Si diode fitted with a KG5 filter to bring the spectral mismatch to unity. The calibration standard was calibrated by the National Renewable Energy Laboratory (NREL). The incident photon-to-current efficiency (IPCE) (Mc science) was measured against the best-performance device. All devices were encapsulated and stored in air for 600 h in the dark for investigation of the long-term stability (Test ID: ISOS-D-1Shelf) [28].

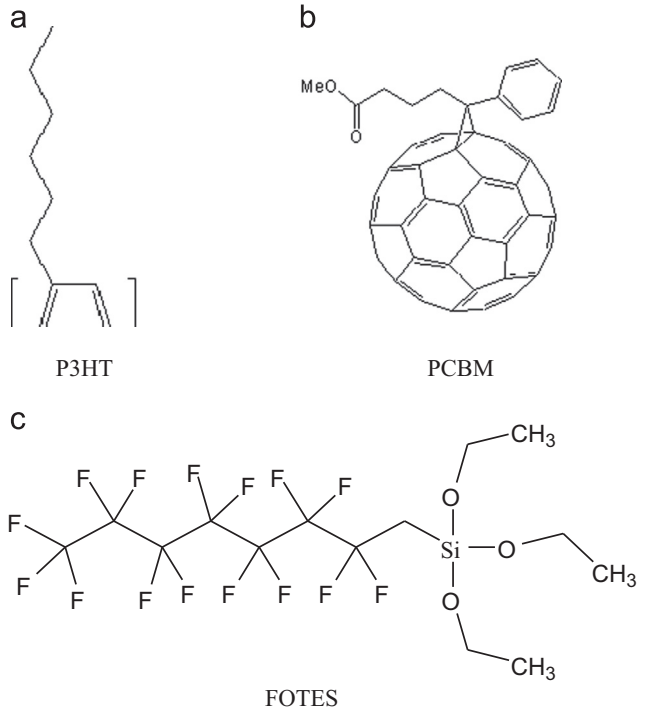

Fig. 1. Chemical structure of (a) P3HT, (b) PCBM and (c) FOTES.

3. Experimental

3.1. Cleaning of patterned ITO glass

To clean the patterned ITO glass, it was sonicated for 20 min. sequentially in detergent (Alconox® in deionized water, 10%), acetone, isopropyl alcohol, and deionized water. The moisture was thoroughly removed by N_2 gas flow. To ensure complete removal of all of the remaining water, the patterned ITO glass was heated on a hot plate for 10 min at 100 °C. For hydrophilic treatment of the patterned ITO glass, it was cleaned for 10 min in a UVO cleaner.

3.2. SAM formation on ITO

FOTES (5 mM) and nitric acid (0.01 M) were mixed at a 100:1 M ratio. The mixed solution was used after being filtered with a 0.2-μm PTFE syringe filter. To form an OH group on the surface of the patterned ITO glass, UVO cleaning was performed for 30 min. After applying 0.4 ml of FOTES solution to the patterned ITO glass, it was kept on a petri dish at 25 °C for 17 h. Then, it was sonicated with isopropyl alcohol for 3 min and annealed at 90 °C on a hot plate in an N_2-filled glove box.

3.3. Fabrication of PSCs

To produce a conventional cell, an aqueous solution of PEDOT:PSS was spin-coated to form a 40-nm-thick film on the patterned ITO glass. The substrate was dried for 10 min at 140 °C in air and then transferred into a glovebox to spin coat the active layer. A solution containing a mixture of P3HT/ PCBM (1:0.6) in ODCB was then spin-coated on top of the PEDOT:PSS to produce a 130-nm-thick photoactive layer, which was then subjected to thermal annealing at 160 °C for 10 min. To form the metal cathode, Al (5 Å/s, 100 nm) was thermally deposited in a high-vacuum ($<10^{-7}$ Torr) chamber.

For the FOTES-ITO-based PSC, photo-active ink was then spin-coated on top of the FOTES-ITO to produce a 130-nm-thick photoactive layer, which was then thermally annealed at 160 °C for 10 min. The method of forming the metal electrode was the same as that for the conventional cell.

4. Results and discussion

Fig. 2 shows the *J–V* curve and IPCE data of the PSCs fabricated with FOTES–ITO, ITO/PEDOT:PSS, and ITO with no surface treatment. The results are presented in Table 1. The PCE of the FOTES–ITO-based PSC was 3.4%, showing better efficiency than the device in which PEDOT:PSS was used as an anode buffer layer. This result was

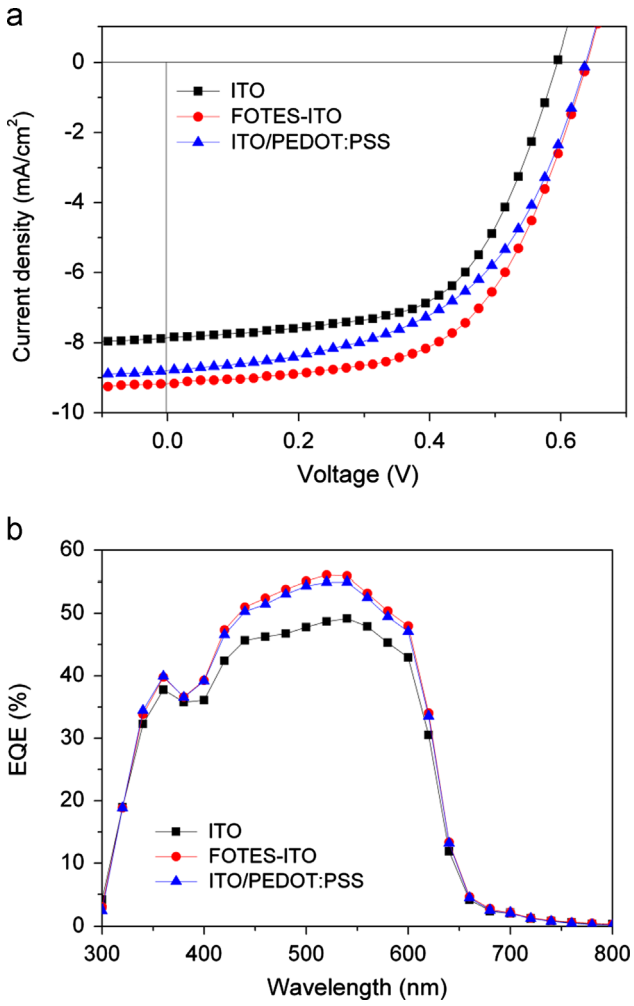

Fig. 2. (a) *J–V* characteristics and (b) external quantum efficiency (EQE) characteristics of PSCs with various anode configurations.

Table 1
Photovoltaic performance of various anode configurations.

Anode	J_{SC} [mA/cm^2]	V_{OC} [V]	FF [%]	PCE [%]	R_S [Ω cm^2]	R_{SH} [Ω cm^2]
ITO	7.8	0.59	48.5	2.3	17.1	714
FOTES–ITO	9.2	0.63	57.9	3.4	16.4	789
ITO/PEDOT:PSS (40 nm)	8.8	0.63	53.2	3.0	16.5	767

Anode/P3HT:PCBM(1:0.6, 130 nm)/BaF_2 (2 nm)/Ba (2 nm)/Al (100 nm).

obtained because (i) FOTES had no effect in terms of transmittance, (ii) the work function of ITO changed with the change in the hole injection barrier, and (iii) the morphology of the photo-active layer changed with the change in the characteristics of the ITO surface after the introduction of FOTES.

The transmittance data of ITO and FOTES–ITO are shown in Fig. 3. Because there was almost no change in the transmittance between the two samples, it has been confirmed that the FOTES SAM is appropriate for the surface modification of ITO. Fig. 4 shows the UPS spectra of ITO and FOTES–ITO. Using this information, the work functions were calculated. The work function of ITO was 4.4 eV, while that of FOTES–ITO was 5.2 eV (an increase of 0.8 eV compared to ITO). As the work function of FOTES-ITO approached the HOMO level of the PCBM acceptor, the hole injection barrier decreased. As a result, the short circuit current density (J_{SC}) increased compared to the device to which PEDOT:PSS was applied.

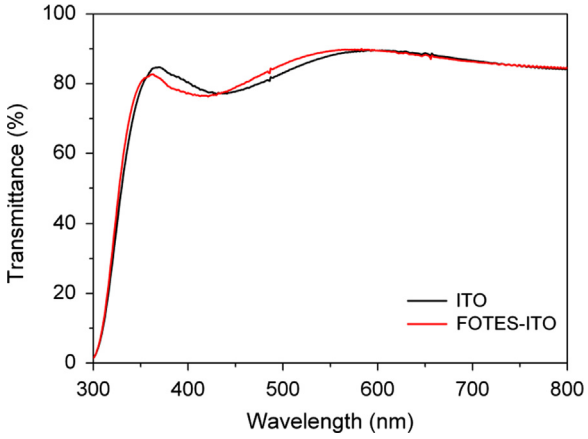

Fig. 3. Transmittance data of ITO and FOTED–ITO.

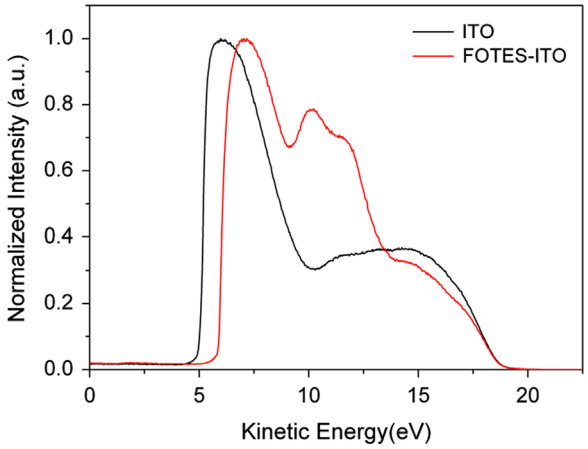

Fig. 4. UPS spectra of ITO and FOTES–ITO.

Fig. 5 shows the measurement of contact angles of ITO and FOTES–ITO. Fig. 5(a) and (b) show the UVO-treated ITO sample, and the sample in which the FOTES SAM was formed on the ITO surface after applying one drop of DI water to each. After the UVO treatment, the ITO surface was changed to hydrophilic. As a result, it showed a contact angle of ca. 10°. On the surface of FOTES–ITO, however, the contact angle increased to ca. 120°, because of the hydrophobic fluorine group. Hence, it has been confirmed that a FOTES monolayer was perfectly formed on the ITO surface.

Fig. 6(a) and (b) show the surface morphologies of ITO and FOTES–ITO, which were observed through AFM. The root mean square (RMS) roughnesses of the two samples were 3.85 nm and 3.84 nm, respectively, confirming that a homogeneous SAM layer was formed on the ITO. Fig. 5(c) and (d) show the surface morphologies of the P3HT:PCBM layer, which was spin-coated onto the ITO and FOTES–ITO. The RMS roughness of the P3HT:PCBM coated onto the ITO surface was 5.84 nm, while that of P3HT:PCBM spin-coated on the FOTES–ITO was 4.43 nm. This result was obtained because of the hydrophobic characteristics of the P3HT:PCBM solution. A rough morphology was observed since, an inhomogeneous film was formed on the hydrophilic ITO surface. However, FOTES–ITO was better than ITO in terms of morphology, with hydrophobic characteristics.

As shown in Table 1, the shunt resistance (R_{SH}) of the device with PEDOT:PSS introduced was 767 Ω cm^2, while that of the FOTES–ITO-based device was 789 Ω cm^2. With the introduction of FOTES, the surface morphology of P3HT:PCBM was improved. In addition, FF increased, because of the decrease in the charge recombination of the P3HT:PCBM layer and the Al interface [29].

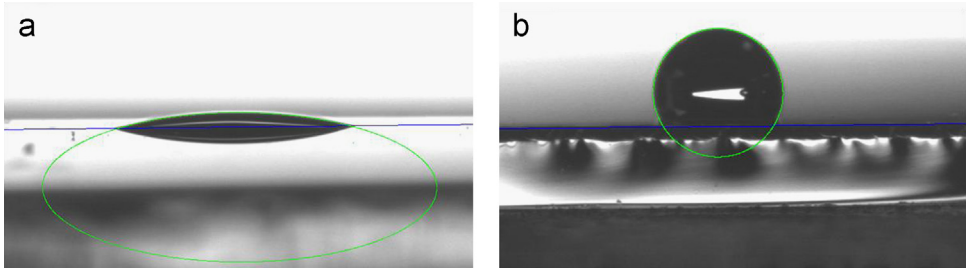

Fig. 5. Pictures of a drop of DI water on the surface of (a) ITO and (b) FOTES–ITO.

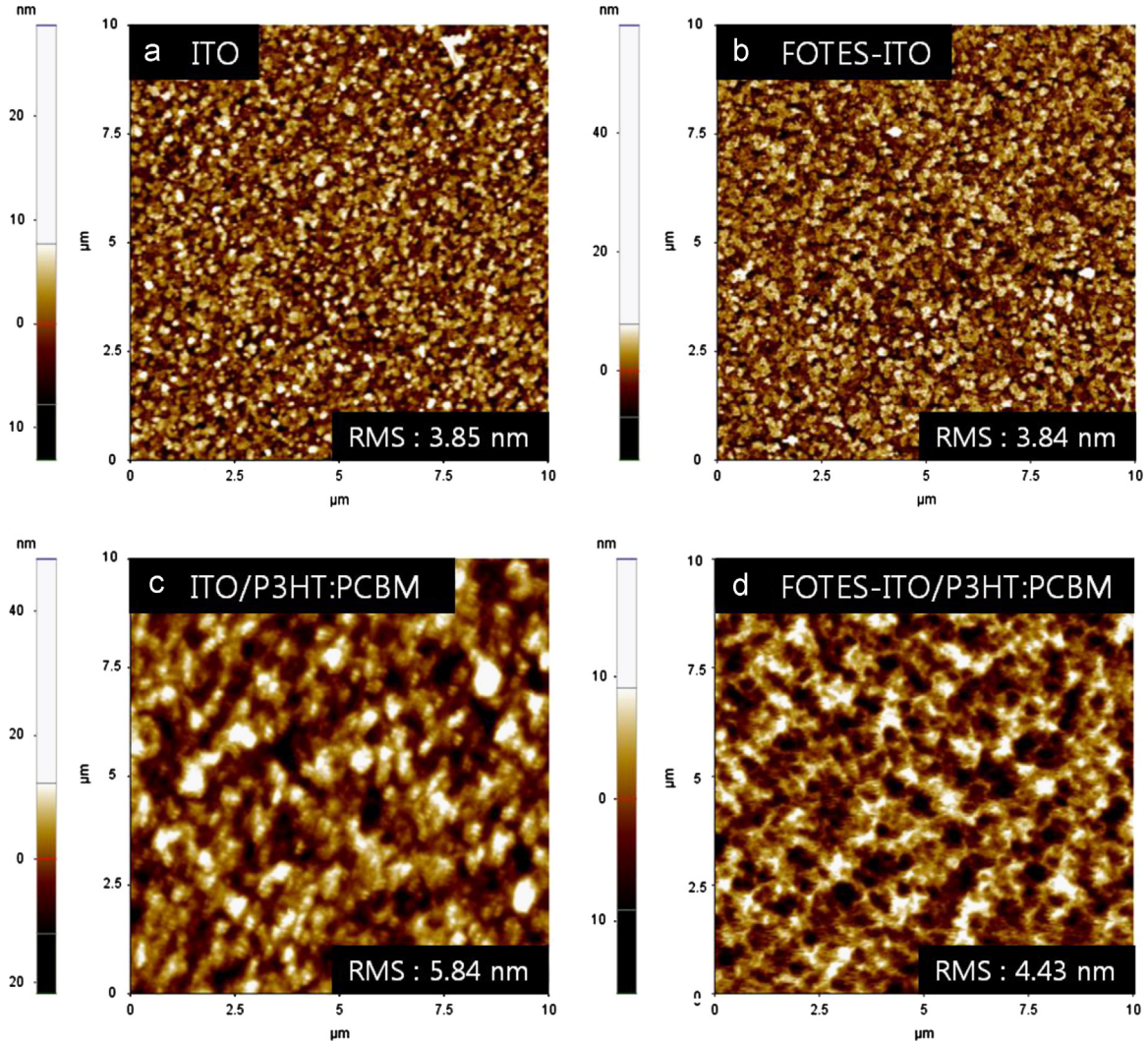

Fig. 6. AFM images of the surfaces of (a) ITO, (b) FOTES–ITO, (c) ITO/P3HT:PCBM and (d) FOTES–ITO/P3HT:PCBM.

In addition, the increase in the surface morphology of P3HT:PCBM and enhancement of the work function in the ITO slightly reduced the series resistance (R_S) by reducing the internal resistance and hole injection barrier of the device. As a result, J_{SC} increased from 8.8 mA/cm^2 to 9.2 mA/cm^2.

Fig. 7 shows how the homogeneous FOTES SAM is formed on the ITO surface. For the effective formation of FOTES on the ITO surface, the ITO surface was modified with a hydroxyl group after UVO cleaning (Fig. 7(b)). If nitric acid is added to FOTES at a 100:1 M ratio, a condensation reaction could take place among ethoxy groups. Therefore, a homogeneous SAM could be formed, as shown in Fig. 7(d).

Fig. 8 shows the result of the stability test on the PSCs to which PEDOT:PSS and FOTES–ITO were applied. All devices were encapsulated and kept in air for 600 h. In the FOTES–ITO-based devices, 36% degradation was observed after 600 h. In the devices with PEDOT:PSS applied, the PCE decreased to one fifth of the original level. It has been confirmed that the long-term stability was increased through the introduction of FOTES to the ITO and through the elimination of the PEDOT:PSS layer.

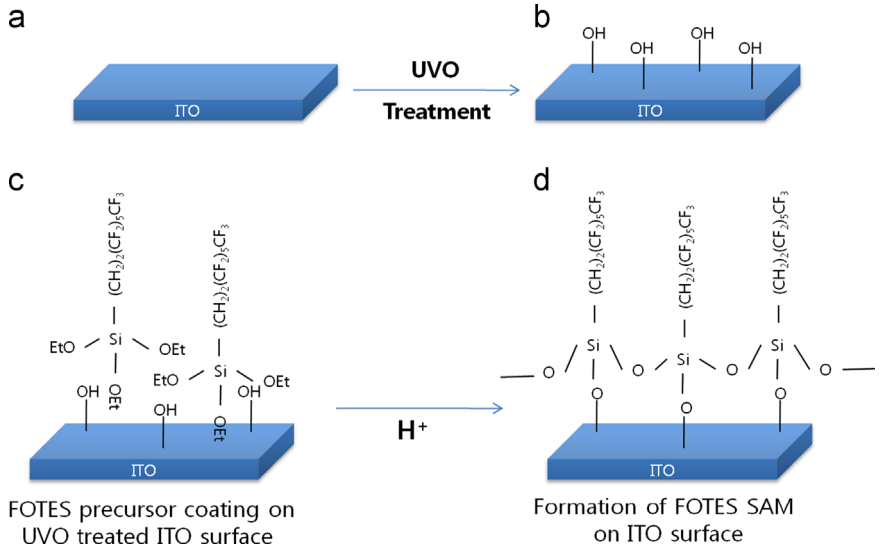

Fig. 7. Mechanism of FOTES attachment to ITO surface. (a) Bare ITO, (b) hydroxyl group coated onto the ITO surface by UV-ozone treatment, (c) FOTES precursor coated onto the UVO-treated ITO surface, and (d) formation of homogeneous FOTES SAM on the ITO surface by adding nitric acid.

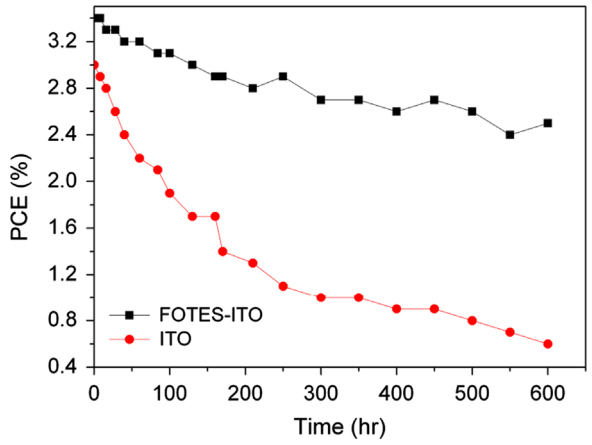

Fig. 8. PCE as a function of storage time for conventional PSC and FOTES–ITO-based PSCs.

5. Conclusions

To enhance the PCE and stability, FOTES was introduced as a SAM material in solution-processable PSCs by modifying ITO. With the formation of a SAM in ITO, the ITO surface became hydrophobic. Then, the morphology of the active layer was improved by increasing the wettability of the hydrophobic P3HT:PCBM solution. In addition, the hole injection barrier was lowered by increasing the work functions of ITO. Consequently, the J_{SC} and FF values were enhanced with the decrease of R_S and the increase of R_{SH}. As a result, a PCE of 3.4% was observed without PEDOT:PSS. In addition, the in-air stability was enhanced by a factor of more than three compared to the device with the PEDOT:PSS layer.

Acknowledgement

This research was supported by a grant(10037195) from the Fundamental R&D Program for Core Technology of Materials funded by the Ministry of Knowledge Economy, Republic of Korea and the technology supporting project grant funded by the Korea government Ministry of Knowledge Economy (No.2012K10042360).

References

[1] J.Y. Lee, Y.J. Kwon, J.W. Woo, D.K. Moon, Synthesis and characterization of fluorene-thiophene based π-conjugated polymers using coupling reaction, Journal of Industrial and Engineering Chemistry 14 (2008) 810–817.
[2] H.J. Song, D.H. Kim, E.J. Lee, S.W. Heo, J.Y. Lee, D.K. Moon, Conjugated polymer consisting of quinacridone and benzothiadiazole as donor materials for organic photovoltaics: coplanar property of polymer backbone, Macromolecules 45 (2012) 7815.
[3] D.H. Yun, H.S. Yoo, S.W. Heo, H.J. Song, D.K. Moon, J.W. Woo, Y.S. Park, Synthesis and photovoltaic characterization of D/A structure compound based on N-substituted phenothiazine and benzothiadiazole, Journal of Industrial and Engineering Chemistry 19 (2013) 421-426, http://dx.doi.org/10.1016/j.jiec.2012.08.033.
[4] H.-Y. Chen, J.H. Hou, S.Q. Zhang, Y.Y. Liang, G.W. Yang, Y. Yang, L.P. Yu, Y. Wu, G. Li, Polymer solar cells with enhanced open-circuit voltage and efficiency, Nature Photonics 3 (2009) 649.
[5] Y. Liang, Z. Xu, J. Xia, S.-T. Tsai, Y. Wu, G. Li, C. Ray, L. Yu, For the bright future bulk heterojunction polymer solar cells with power conversion efficiency of 7.4%, Advanced Materials 22 (2010) E135.
[6] F.C. Krebs, Fabrication and processing of polymer solar cells: A review of printing and coating techniques, Solar Energy Materials and Solar Cells 93 (2009) 394.
[7] E. Bundgaard, O. Hagemann, M. Manceau, M. Jørgensen, Low band gap polymers for roll-to-roll coated polymer solar cells, Macromolecules 43 (2010) 8115.
[8] M. Manceau, D. Angmo, M. Jørgensen, F.C. Krebs, ITO-free flexible polymer solar cells: from small model devices to roll-to-roll processed large modules, Organic Electronics 12 (2011) 566.
[9] F.C. Krebs, J. Fyenbo, M. Jørgensen, Product integration of compact roll-to-roll processed polymer solar cell modules: methods and manufacture using flexographic printing, slot-die coating and rotary screen printing, Journal of Materials Chemistry 20 (2010) 8994.
[10] S.W. Heo, J.Y. Lee, H.J. Song, J.R. Ku, D.K. Moon, Patternable brush painting process for fabrication of flexible polymer solar cells, Solar Energy Materials and Solar Cells 95 (2011) 3041.
[11] S.W. Heo, K.W. Song, M.H. Choi, T.H. Sung, D.K. Moon, Patternable solution process for fabrication of flexible polymer solar cells using PDMS, Solar Energy Materials and Solar Cells 95 (2011) 3564.
[12] Z. He, C. Zhong, X. Huang, W.-Y. Wong, H. Wu, L. Chen, S. Su, Y. Cao, Simultaneous enhancement of open-circuit voltage, short-circuit current density, and fill factor in polymer solar cells, Advanced Materials 23 (2011) 4636.
[13] Z. He, C. Zhong, S. Su, M. Xu, H. Wu, Y. Cao, Enhanced power-conversion efficiency in polymer solar cells using an inverted device structure, Nature Photonics 6 (2012) 591.
[14] A. Wicklein, S. Ghosh, M. Sommer, F. Wurthner, M. Thelakkat, Self assembly of semiconductor organogelator nanowires for photoinduced charge separation, ACS Nano 3 (2009) 1107.
[15] M. Jorgensen, K. Norrman, F.C. Krebs, Stability/degradation of polymer solar cells, Solar Energy Materials and Solar Cells 92 (2008) 686.
[16] T. Oyamada, C. Maeda, H. Sasabe, C. Adachi, Efficient electron injection mechanism in organic light-emitting diodes using an ultra thin layer of low-work-function metals, Japanese Journal of Applied Physics 42 (2003) L1535.

[17] G. Li, C.W. Chu, V. Shrotriya, J. Huang, Y. Yang, Efficient inverted polymer solar cells, Applied Physics Letters 88 (2006) 253503.
[18] M.P. de Jong, L.J. van Ijzendoorn, M.J.A. de Voigt, Stability of the interface between indium-tin-oxide and poly(3,4-ethylenedioxythiophene)/poly(styrenesulfonate) in polymer light-emitting diodes, Applied Physics Letters 77 (2000) 2255.
[19] I.S. Song, S.W. Heo, J.H. Lee, J.R. Haw, D.K. Moon, Study on the ClO_4 doped PEDOT-PEG in organic solvent using a hole injection layer for PLEDs, Journal of Industrial and Engineering Chemistry 17 (2011) 651.
[20] I.S. Song, S.W. Heo, J.R. Ku, D.K. Moon, Study on the antimony tin oxide as a hole injection layer for polymer light emitting diodes, Thin Solid Films 520 (2012) 4068.
[21] M.G. Helander, Z.B. Wang, J. Qiu, M.T. Greiner, D.P. Puzzo, Z.W. Liu, Z.H. Lu, Chlorinated indium tin oxide electrodes with high work function for organic device compatibility, Science 332 (2011) 944.
[22] K. Sun, J. Ouyang, Polymer solar cells using chlorinated indium tin oxide electrodes with high work function as the anode, Solar Energy Materials and Solar Cells 96 (2012) 238.
[23] M. Cerruti, C. Rhodes, M. Losego, A. Efremenko, J.P. Maria, D. Fischer, S. Franzen, J. Genzer, Influence of indium–tin oxide surface structure on the ordering and coverage of carboxylic acid and thiol monolayers, Journal of Physics D: Applied Physics 40 (2007) 4212.
[24] J. Ouyang, C.W. Chu, C. Szmanda, L. Ma, Y. Yang, Programmable polymer thin film and nonvolatile memory device, Nature Materials 3 (2004) 918.
[25] J.S. Kim, J.H. Park, J.H. Lee, J. Jo, D.Y. Kim, Control of the electrode work function and active layer morphology via surface modification of indium tin oxide for high efficiency organic photovoltaics, Applied Physics Letters 91 (2007) 112111.
[26] A. Tada, Y. Geng, M. Nakamura, Q. Wei, K. Hashimoto, K. Tajima, Interfacial modification of organic photovoltaic devices by molecular self-organization, Physical Chemistry Chemical Physics 14 (2012) 3713.
[27] A. Sharma, A. Haldi, W.J. Potscavage Jr., P.J. Hotchkiss, S.R. Marderb, B. Kippelen, Effects of surface modification of indium tin oxide electrodes on the performance of molecular multilayer organic photovoltaic devices, Journal of Materials Chemistry 19 (2009) 5298.
[28] M.O. Reese, S.A. Gevorgyan, M. Jørgensen, E. Bundgaard, S.R. Kurtz, D.S. Ginley, D.C. Olson, M.T. Lloyd, P. Morvillo, E.A. Katz, A. Elschner, O. Haillant, T. R. Currier, V. Shrotriya, M. Hermenau, M. Riede, K.R. Kirov, G. Trimmel, T. Rath, O. Inganäs, F. Zhang, M. Andersson, K. Tvingstedt, M. Lira-Cantu, D. Laird, C. McGuiness, S. Gowrisanker, M. Pannone, M. Xiao, J. Hauch, R. Steim, D.M. DeLongchamp, R. Rösch, H. Hoppe, N. Espinosa, A. Urbina, G. Yaman-Uzunoglu, J.-B. Bonekamp, A.J.J.M. van Breemen, C. Girotto, E. Voroshazi, F.C. Krebs, Consensus stability testing protocols for organic photovoltaic materials and devices, Solar Energy Materials and Solar Cells 95 (2011) 1253.
[29] X. Yang, J. Loos, S.C. Veenstra, W.J.N. Verhees, M.M Wienk, J.M. Kroon, M.A. J. Michels, R.A.J. Janssen, Nanoscale morphology of high-performance polymer solar cells, Nano Letters 5 (2005) 579.